ELSEVIER

Effect of axial strain cycling on the critical current density and *n*-value of ITER niobium–tin wires

D.M.J. Taylor, D.P. Hampshire *

Superconductivity Group, Department of Physics, University of Durham, South Road, Durham DH1 3LE, UK

Abstract

Measurements have been made of the effect of axial strain cycling on the critical current density and *n*-value of two ITER candidate niobium–tin wires (Europa Metalli-LMI (EM-LMI) and Vacuumschmelze). The wires were subjected to ~1300 strain cycles to incrementally increasing applied tensile strains, with 100 cycles per 0.056% increment. For both wires, there were no changes in the critical current density or *n*-value for the ~500 cycles up to 0.282% applied strain (except for the first cycle of the EM-LMI wire). Cycling to higher applied strains (0.339–0.677%) caused the critical current density and *n*-value to incrementally increase at all applied strains, with the critical current density eventually increasing by 5–7% at 12 T and zero intrinsic strain. Cycling to applied strains above 0.677% (~0.4% intrinsic strain) damaged the wires.
© 2003 Elsevier B.V. All rights reserved.

1. Introduction

Strain has a very large effect on the superconducting properties of Nb_3Sn. In superconducting magnets, strain arises from the differential thermal contraction that occurs on cooling to cryogenic temperatures, and the Lorentz-forces that occur during high-field operation. The International Thermonuclear Experimental Reactor (ITER) will use magnets made from cable-in-conduit conductors (CICCs) with Nb_3Sn strands (wires) [1]. For

these large-scale high-field magnets, knowledge of the effects of strain is extremely important. In addition, the ITER magnets will undergo many charging cycles (up to 50,000), and so the effects of cyclic strain and fatigue also need to be considered.

The axial-strain dependence of the critical current density [2–4] (and *n*-value [5]) of technical Nb_3Sn wires has been measured extensively. The effects are generally found to be reversible, to first order, for small numbers of cycles over quite large ranges of strain, while at higher strains damage occurs to the superconducting filaments. However, the effects of large numbers of strain cycles within the so-called reversible regime has not been widely investigated. A study of bronze-route Nb_3Sn wires stress cycled at room-temperature did not observe fatigue effects [6], nor did a study of CICCs subject

---
* Corresponding author. Tel.: +44-191-3343654; fax: +44-191-3345823.
E-mail address: d.p.hampshire@dur.ac.uk (D.P. Hampshire).
URL: http://www.dur.ac.uk./superconductivity.durham.

to axial strain cycles at cryogenic temperatures [7]. In contrast, investigations of transverse stress cycling of CICCs [8] and cyclic charging of ITER model coils [1] have found some evidence of fatigue effects and in order to understand these results, accurate data for the component wires are required. The work presented in this paper is the first reported investigation of the effects of axial strain cycling (involving >1000 cycles) at cryogenic temperatures on the critical current density and n-value of technical Nb_3Sn wires.

2. Experimental

Measurements were made on two different 0.81 mm diameter ITER candidate Nb_3Sn wires: an internal-tin wire made by Europa Metalli-LMI (EM-LMI) and a bronze-route wire made by Vacuumschmelze (VAC). The wires were heat-treated in an argon atmosphere on (oxidised) stainless steel mandrels as follows: 570 °C for 220 h and 650 °C for 175 h for the VAC wire; 210 °C for 100 h, 340 °C for 24 h, 450 °C for 18 h and 650 °C for 200 h for the EM-LMI wire. The chromium plating was then removed using hydrochloric acid, and the wires were transferred to copper–beryllium spring sample-holders, and attached by copper-plating and soldering. Axial strain was then applied to the wire by twisting one end of the spring with respect to the other [9]. The springs had tee-shaped cross-sections designed to minimise the strain gradient across the wire [10].

The experiments were carried out using our strain probe [11] with an added computer-controlled stepper motor (see Fig. 1). This enables strains (and strain cycles) to be applied automatically, with a resolution of ∼10^{-6}% strain per step. Voltage–current (V–I) measurements were made at 4.2 K with the wire immersed in a liquid-helium bath. These involved slowly increasing the current, and measuring the voltages across three different sections of the wire using nanovolt amplifiers and digital voltmeters. The experiments consisted of single strain-cycles during which V–I measurements were made (test cycles), alternated with sets of 100 strain cycles (see Fig. 2). The maximum applied strain was increased for each successive set
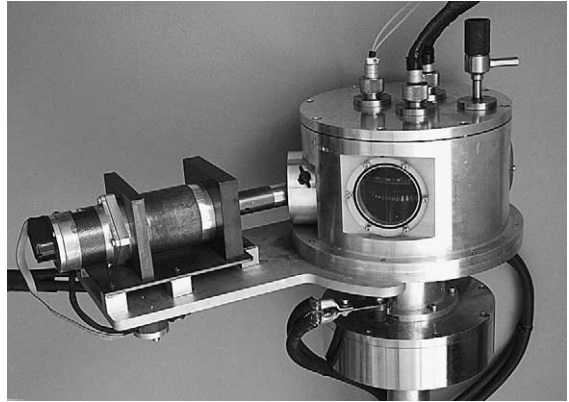

Fig. 1. The top end of the strain probe, with the computer-controlled stepper motor (on the left).
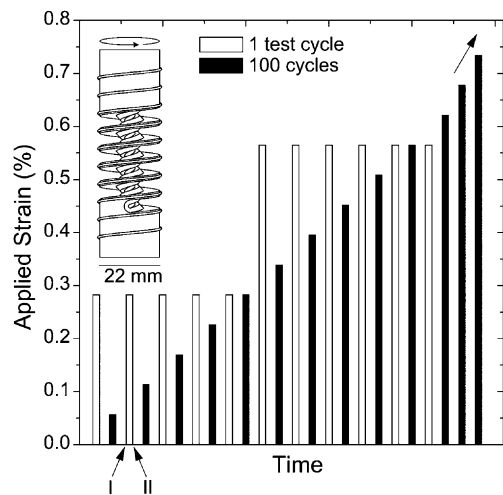

Fig. 2. The strain cycling procedure. The labels I and II refer to the measurements at zero applied strain at the beginning and the end of each test cycle respectively. Inset: spring sample holder with tee-shaped cross-section.

of 100 cycles in increments of 0.056% until the wire was damaged. The test cycles were first carried out to 0.282% applied strain and after the set of 100 cycles to 0.282% had been completed, they were then carried out to 0.565%. V–I measurements were made at magnetic fields between 9 and 15 T at zero applied strain at the beginning of the test cycle, at 10 and 12 T during the first half of the cycle and then at 10 and 12 T at zero applied strain

at the end of the cycle. No test cycles were carried out after sets of cycles to applied strains above 0.565%, but measurements were made at 10 and 12 T during the 100th cycle, at the maximum applied strain and at zero applied strain. The strain was changed at a constant maximum speed of 0.008% s^{-1} (e.g. cycles to 0.282% had a time-period of ∼90 s). In addition, the temperature of the wire was kept below ∼20 K for the entire experiment (the VAC wire was subjected to a thermal cycle to room temperature after strain cycling to 0.565%, but this had no significant effect).

3. Results

Fig. 3 shows the electric field–engineering current density (E–$J_{(E)}$) characteristics for the three different sections of the EM-LMI wire (A, B and C) at zero applied strain before any cycling. E and $J_{(E)}$ were calculated from the voltage and current by dividing by the voltage-tap separation (typically ∼20 mm) and the cross-sectional area of the wire (5.15×10^{-7} m^2). The data are typical of both wires, which were homogeneous in terms of their

E–$J_{(E)}$ characteristics to within 5% (until damage occurred). This paper will consider engineering critical current densities ($J_{C(E)}$) defined at an electric-field criterion of 10 μV m^{-1} and n-values calculated using $E = \alpha J_{(E)}^{n}$ for the electric-field range 10–100 μVm^{-1}. $J_{C(E)}$ and n clearly depend on the choice of criterion (e.g. n typically varies by 50% in the experimentally accessible electric-field range 1–1000 μV m^{-1}, decreasing with increasing E), but the trends described below do not depend on this choice.

3.1. EM-LMI wire

Figs. 4 and 5 show the engineering critical current density and n-value for the EM-LMI wire as a function of applied strain (ε), measured after each set of 100 strain cycles. Data are shown for one section of the wire (A) at a magnetic field of 12 T, but the same trends were observed for the other sections and at 10 T. Figs. 6 and 7 show the $J_{C(E)}$ and n data at zero applied strain and 12 T, measured after each set of 100 strain cycles before and after each test cycle. The first test-cycle to 0.282% applied strain caused a 1% decrease in $J_{C(E)}$ at $\varepsilon = 0\%$ for all three sections of the wire (for n, the experimental errors are too large to observe
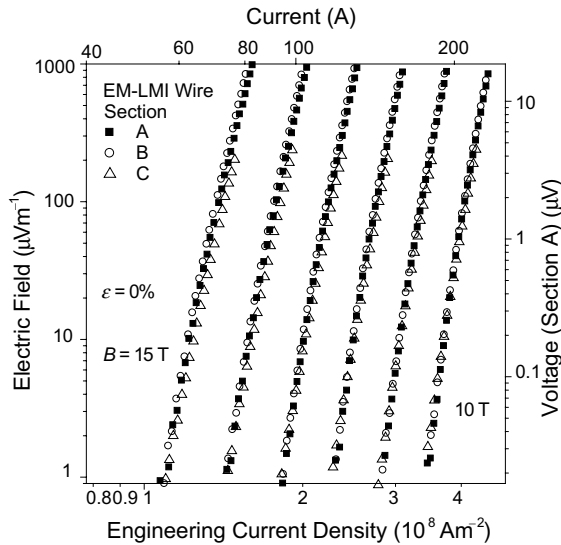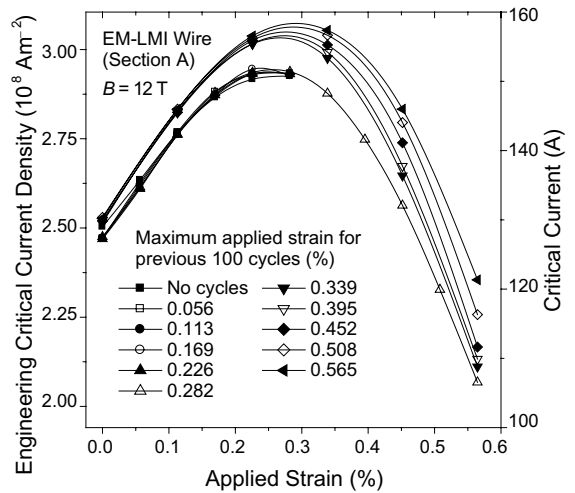
Fig. 3. Electric field versus engineering current density (and voltage versus current) on a log–log scale for three different sections of the EM-LMI wire at zero applied strain (before any cycling) and integer magnetic fields between 10 and 15 T.

Fig. 4. Engineering critical current density (and critical current) defined at 10 μV m^{-1} as a function of applied strain for section A of the EM-LMI wire at a magnetic field of 12 T, measured after each set of 100 strain cycles.
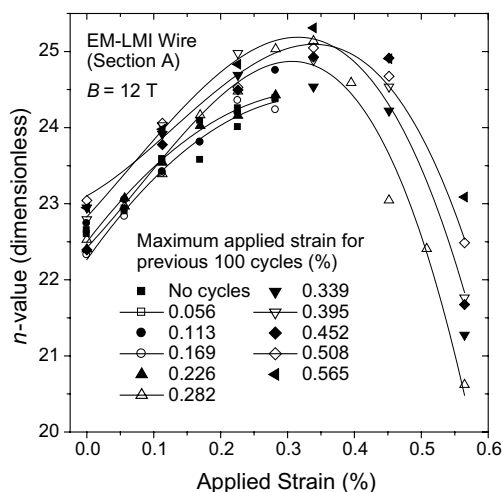
Fig. 5. *n*-value as a function of applied strain for section A of the EM-LMI wire at a magnetic field of 12 T, measured after each set of 100 strain cycles. The *n*-value was calculated for the electric field range 10–100 μV m^{-1}.
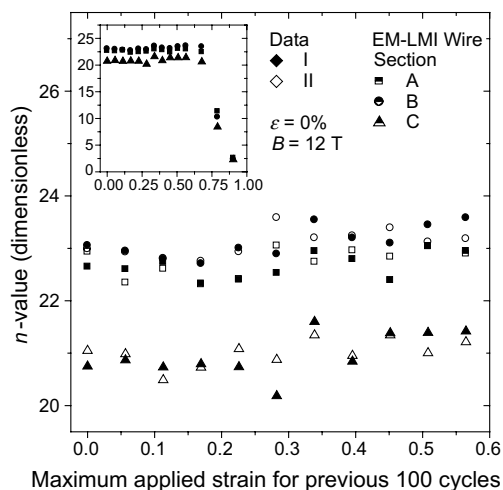

Fig. 7. *n*-value for three different sections of the EM-LMI wire at zero applied strain and a magnetic field of 12 T, plotted as a function of the maximum applied strain for the previous 100 cycles. Data are shown at the beginning (I) and at the end (II) of the single test-cycles. Inset: data (I) for all applied strains.
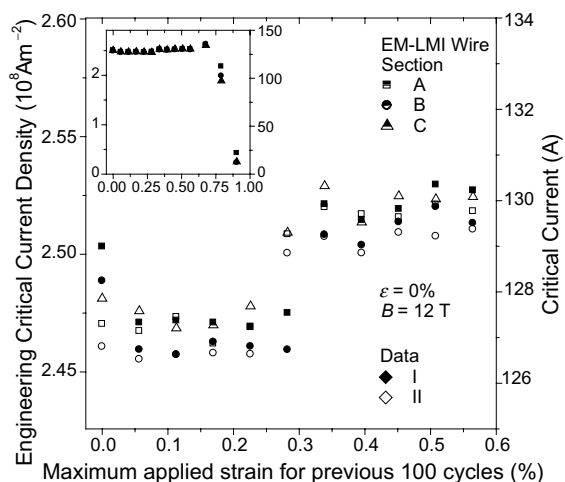

Fig. 6. Engineering critical current density (and critical current) for three different sections of the EM-LMI wire at zero applied strain and a magnetic field of 12 T, plotted as a function of the maximum applied strain for the previous 100 cycles. Data are shown at the beginning (I) and at the end (II) of the single test-cycles. Inset: data (I) for all applied strains.

and *n* are a maximum at $\varepsilon = \varepsilon_{\mathrm{M}} = 0.26\%$ with values of 2.95×10^8 A m^{-2} (152 A) and 24.5 respectively. The first test-cycle to $\varepsilon = 0.565\%$ caused $J_{\mathrm{C(E)}}$ at zero applied strain to increase by $\sim 2\%$. At low applied strains ($\leqslant 0.226\%$), $J_{\mathrm{C(E)}}$ (and *n*) were then unaffected by the subsequent ~ 500 cycles to applied strains between 0.339% and 0.565%. However, at high applied strains ($\geqslant 0.226\%$) these multiple cycles caused $J_{\mathrm{C(E)}}$ and *n* to increase after each successive set of cycles (approximately monotonically), resulting in a final increase in $J_{\mathrm{C(E)}}$ at $\varepsilon = \varepsilon_{\mathrm{M}}$ of 5% as well as a small increase in ε_{M} itself to 0.29%. The increases were proportionally larger at higher applied strains ($\sim 14\%$ at $\varepsilon = 0.565\%$). Cycling to $\varepsilon = 0.677\%$ caused $J_{\mathrm{C(E)}}$ at zero applied strain to increase by a further 2.5% (no test cycle was carried out). Finally, cycling to $\varepsilon = 0.790\%$ caused $J_{\mathrm{C(E)}}$ and *n* at zero applied strain to reduce by 15% and 50% respectively, indicating damage to the wire. Further damage occurred after cycling to $\varepsilon = 0.903\%$.

3.2. VAC wire

Equivalent data for the VAC wire are shown in Figs. 8–11. The scatter on the data is generally

changes of this magnitude). For subsequent cycles to applied strains up to and including 0.282% (~ 500 cycles in total), the data were reversible to within the experimental error. In this regime, $J_{\mathrm{C(E)}}$
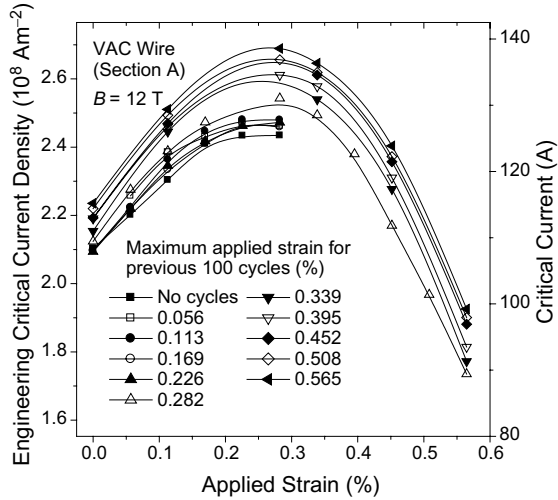
Fig. 8. Engineering critical current density (and critical current) as a function of applied strain for section A of the VAC wire at a magnetic field of 12 T, measured after each set of 100 strain cycles.

Fig. 10. Engineering critical current density (and critical current) for three different sections of the VAC wire at zero applied strain and a magnetic field of 12 T, plotted as a function of the maximum applied strain for the previous 100 cycles. Data are shown at the beginning (I) and at the end (II) of the single test-cycles. Inset: data (I) for all applied strains.
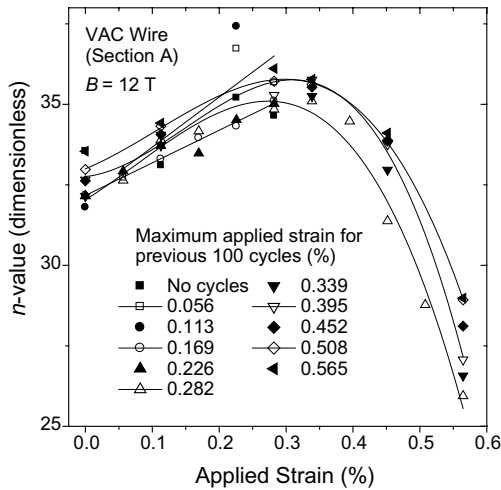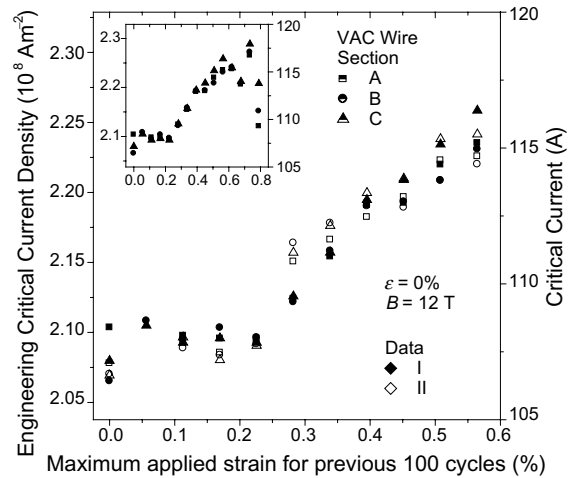

Fig. 9. *n*-value as a function of applied strain for section A of the VAC wire at a magnetic field of 12 T, measured after each set of 100 strain cycles.

Fig. 11. *n*-value for three different sections of the VAC wire at zero applied strain and a magnetic field of 12 T, plotted as a function of the maximum applied strain for the previous 100 cycles. Data are shown at the beginning (I) and at the end (II) of the single test-cycles. Inset: data (I) for all applied strains.
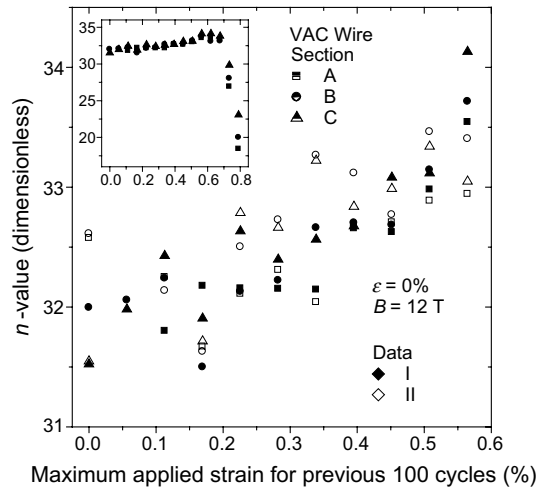
larger, but $J_{C(E)}$ and n are again reversible to within the experimental error for cycles to applied strains up to 0.282% (no irreversible effect due to the first cycle was observed for this wire). In this case $J_{C(E)} = 2.5 \times 10^8 \, \mathrm{A \, m^{-2}}$ (128 A) and $n = 35$ at

$\varepsilon = \varepsilon_{\mathrm{M}} = 0.26\%$ and 12 T. $J_{C(E)}$ and n again increased after each successive set of cycles to

applied strains between 0.339% and 0.565%, with $J_{C(E)}$ at $\varepsilon = \varepsilon_M$ and 12 T increasing by 7% in total. This was similar to the EM-LMI wire, except that at low applied strains ($\leqslant 0.113\%$) larger increases occurred ($J_{C(E)}$ increased by 6% in total at zero applied strain) and there was no indication of a change in ε_M. Evidence of damage from the $J_{C(E)}$ data was first observed after cycling to $\varepsilon = 0.790\%$, although n also decreased considerably (by 25%) after cycling to $\varepsilon = 0.734\%$.

4. Discussion

For engineering purposes, it may be sufficient to know that there were no decreases in the critical current density or n-value for either wire during the >1000 strain cycles to applied strains up to 0.677%. Nevertheless, significant increases in the critical current density and n-value did occur as a result of strain cycling to applied strains between 0.339% and 0.677%. In fact, the increases in $J_{C(E)}$ are associated with increases in the effective upper critical field (Kramer plots not shown), while increases in n are broadly related to increases in $J_{C(E)}$. The brittle Nb_3Sn filaments behave elastically until damage (cracking) occurs at values of intrinsic strain in the range 0.3–0.6% for most wires (compared to $\sim 0.4\%$ in this work), where intrinsic strain is, by convention, taken to be zero where $J_{C(E)}$ is a maximum [12]. The changes in $J_{C(E)}$ and n are therefore likely to be caused by changes in the strain-state of the Nb_3Sn filaments. The copper and bronze matrix materials have elastic limits of $\sim 0.1\%$ and $\sim 0.2\%$ respectively (and are in thermal pretension at zero applied strain), and so will be plastically deformed during strain cycling [12]. In general, loading–unloading treatments on wires can be carried out to reduce the axial thermal prestrain on the filaments [6]. In our experiment, however, the axial strain is directly controlled and therefore the changes in $J_{C(E)}$ and n observed during cycling can only be explained by also considering the non-axial strains. The effects of tensorial strains on Nb_3Sn are not fully understood, although the consensus is that increases in either deviatoric or hydrostatic strain cause the superconducting parameters to decrease, with the devi-

atoric strain (related to the change in shape) having the larger effect [4,13]. This suggests that the increases in $J_{C(E)}$ and n are due to a decrease in one or both of these quantities, although in simple models of wires, if deviatoric strain alone is considered then this is always zero at ε_M (and $J_{C(E)}$ at ε_M is always the same). Detailed knowledge of the complex effects associated with plastic deformation and work hardening of the components of the matrix requires finite element analysis modelling, which is in progress.

5. Conclusions

The results of our measurements of the effect of axial strain cycling on two ITER candidate Nb_3Sn wires (EM-LMI and VAC) can be summarised as follows:

1. Both wires were unaffected by the ~ 500 strain cycles to applied strains up to 0.282% (apart from a 1% decrease in the critical current density caused by the first test-cycle for the EM-LMI wire).
2. The first test-cycle to 0.565% caused a 1–2% increase in the critical current density at zero applied strain (for the EM-LMI wire, this was the only increase in the zero applied strain data during the first ~ 1000 cycles).
3. The ~ 500 strain cycles to applied strains between 0.339% and 0.565% caused the critical current density and n-value to incrementally increase at all applied strains; the final increases were proportionally larger at higher strains and varied from 2% to 14% (EM-LMI wire) and 6% to 11% (VAC wire).
4. Cycling to applied strains above 0.677% ($\sim 0.4\%$ intrinsic strain) caused large irreversible decreases in the critical current density and n-value.

References

[1] N. Mitchell, SOFT 2002, Helsinki, 2002.

[2] J.W. Ekin, Cryogenics 20 (1980) 610.

[3] B. ten Haken, A. Godeke, H.H.J. ten Kate, J. Appl. Phys. 85 (1999) 3247.

[4] N. Cheggour, D.P. Hampshire, Cryogenics 42 (2002) 299.

[5] D.M.J. Taylor, S.A. Keys, D.P. Hampshire, Physica C 372 (2002) 1291.

[6] S. Ochiai, K. Osamura, Cryogenics 32 (1992) 584.

[7] W. Specking, J.L. Duchateau, P. Decool, in: Proc. 15th Int. Conf. Magn. Tech., 1998, p. 1210.

[8] P. Bruzzone, A.M. Fuchs, B. Stepanov, G. Vecsey, IEEE Trans. Appl. Supercond. 12 (2002) 516.

[9] C.R. Walters, I.M. Davidson, G.E. Tuck, Cryogenics 26 (1986) 406.

[10] D.M.J. Taylor, D.P. Hampshire, in press.

[11] N. Cheggour, D.P. Hampshire, Rev. Sci. Instrum. 71 (2000) 4521.

[12] G. Rupp, in: M. Suenaga, A.F. Clark (Eds.), Filamentary A15 Superconductors, Plenum Press, New York, 1980, p. 155.

[13] D.O. Welch, Adv. Cryog. Eng. 26 (1980) 48.